Draft version February 10, 2017
Typeset using LaTeX **twocolumn** style in AASTeX61

THE FRB 121102 CAMPAIGN: MULTI-OBSERVATORY RADIO BURST AND IMPLICATIONS FOR THE FRB POPULATION

C. J. Law,[1] J. W. T. Hessels,[2,3] R. S. Wharton,[4] C. G. Bassa,[2] G. C. Bower,[5] S. Burke-Spolaor,[6,7,8] B. J. Butler,[6] T. Cantwell,[9] S. H. Carey,[10] S. Chatterjee,[4] J. M. Cordes,[4] P. Demorest,[6] R. Fender,[11] K. Grainge,[9] J. Hickish,[12,10] V. M. Kaspi,[13] T. J. W. Lazio,[14] M. A. McLaughlin,[7,8] D. Michilli,[2,3] K. Mooley,[11] Y. C. Perrott,[10] S. M. Ransom,[15] N. Razavi-Ghods,[10] M. Rupen,[16] A. Scaife,[9] P. Scott,[17] P. Scholz,[16] A. Seymour,[18,19] L. G. Spitler,[20] S. P. Tendulkar,[13] D. Titterington,[17] and P. K. G. Williams[21]

[1] *Department of Astronomy and Radio Astronomy Lab, University of California, Berkeley, CA 94720, USA*
[2] *ASTRON, Netherlands Institute for Radio Astronomy, Postbus 2, 7990 AA, Dwingeloo, The Netherlands*
[3] *Anton Pannekoek Institute for Astronomy, University of Amsterdam, Science Park 904, 1098 XH Amsterdam, The Netherlands*
[4] *Cornell Center for Astrophysics and Planetary Science and Department of Astronomy, Cornell University, Ithaca, NY 14853, USA*
[5] *Academia Sinica Institute of Astronomy and Astrophysics, 645 N. A'ohoku Place, Hilo, HI 96720, USA*
[6] *National Radio Astronomy Observatory, Socorro, NM 87801, USA*
[7] *Department of Physics and Astronomy, West Virginia University, Morgantown, WV 26506, USA*
[8] *Center for Gravitational Waves and Cosmology, West Virginia University, Chestnut Ridge Research Building, Morgantown, WV 26505*
[9] *Jodrell Bank Centre for Astrophysics, Alan Turning Building, School of Physics & Astronomy ,The University of Manchester, Oxford Road, Manchester M13 9PL, UK*
[10] *Astrophysics Group, Cavendish Laboratory, 19 J. J. Thomson Avenue, Cambridge CB3 0HE, UK*
[11] *Centre for Astrophysical Surveys, University of Oxford, Denys Wilkinson Building, Keble Road, Oxford OX1 3RH, UK*
[12] *Dept of Astronomy and Radio Astronomy Lab, University of California, Berkeley, CA 94720, USA*
[13] *Department of Physics and McGill Space Institute, McGill University, 3600 University St., Montreal, QC H3A 2T8, Canada*
[14] *Jet Propulsion Laboratory, California Institute of Technology, Pasadena, CA 91109, USA*
[15] *National Radio Astronomy Observatory, Charlottesville, VA 22903, USA*
[16] *National Research Council of Canada, Herzberg Astronomy and Astrophysics, Dominion Radio Astrophysical Observatory, P.O. Box 248, Penticton, BC V2A 6J9, Canada*
[17] *University of Cambridge, UK*
[18] *Arecibo Observatory, HC3 Box 53995, Arecibo, PR 00612, USA*
[19] *Max-Planck-Institut für Radioastronomie, Auf dem Hügel 69, Bonn, D-53121, Germany*
[20] *Max-Planck-Institut für Radioastronomie, Auf dem Hügel 69, D-53121 Bonn, Germany*
[21] *Harvard-Smithsonian Center for Astrophysics, Cambridge, MA, USA*

ABSTRACT

The recent precision localization of FRB 121102 has helped identify its host galaxy, measure its distance, and establish it as a member of a truly new class of astrophysical source. We present results of the coordinated observing campaign that made this localization, including the first simultaneous detection of an FRB burst with multiple telescopes. Of the nine bursts detected by the Very Large Array at 3 GHz, four had simultaneous observing coverage at other observatories, and one was detected by the Arecibo Observatory at 1.4 GHz. We show that the burst spectra typically have a broad shape that tapers off on scales of $\sim$ 500 MHz, plus fine spectral structure on MHz-frequency scales. We present the first FRB energy distribution and temporal statistics for FRB 121102 and argue that the whole FRB population is adequately described by a single class similar to FRB 121102. *population models* *slsn* **This source shows that optimal FRB survey strategies should...**

1. INTRODUCTION

Fast Radio Bursts (FRBs) were discovered ten years ago as a millisecond-duration radio transient with an anomalously high dispersion measure (the "Lorimer burst"; Lorimer et al. 2007). Their large dispersion measure (DM) implied that they originated outside of our Galaxy, potentially at cosmological distances, and were orders of magnitude more luminous than any other millisecond radio transient (Thornton et al. 2013). Both their energetics and distance have inspired a wide variety of models and astrophysical applications (e.g., McQuinn 2014; Kulkarni et al. 2014; Connor et al. 2016b; Cordes & Wasserman 2016). However, that potential was limited by the lack of a definitive association of an FRB to an extragalactic host.

This paper is part of a series based on the first localization of an FRB and its unambiguous association to an extragalactic host (Chatterjee et al. 2017; Tendulkar et al. 2017; Marcote et al. 2017). FRB 121102, also known as the "repeating FRB", was first detected in November 2012 by the Arecibo Observatory (Spitler et al. 2014). In mid 2015, new Arecibo observations revealed a series of bursts at the same DM ($\sim$ 559 pc cm^{-3}) and sky position demonstrating that it repeats (Spitler et al. 2016). Beginning in August of 2015, we made the first of nine detections of FRB 121102 with the Very Large Array (Chatterjee et al. 2017) and localized it with a precision of 0.1″. Subsequent radio and optical observing discovered more bursts from FRB 121102 and associated them with a persistent radio and optical source at a redshift of 0.193 with a precision of 0.01" (Tendulkar et al. 2017; Marcote et al. 2017, $\sim$ 40 pc).

FRB 121102 has now been localized four orders of magnitude better than any other FRB and placed at a cosmological distance. Its lookback and luminosity distances are 746 and 972 Mpc, assuming a concordance cosmology with parameters given by Planck Collaboration et al. (2016). This association means that FRB 121102 is orders of magnitude more luminous than any other millisecond transient and that its DM traces both the host and intergalactic medium (Tendulkar et al. 2017). If FRB 121102 is representative of all FRBs, then we should expect them to be useful as probes of the intergalactic medium and their host galaxies. Thus, the confirmation of a cosmological distance for FRB 121102 has begun to fulfil the promise implied by the Lorimer burst.

Although new models of FRB origin have been already been developed (Kashiyama & Murase 2017; Metzger et al. 2017; Zhang 2017; Dokuchaev & Eroshenko 2017), we still do not know what causes them. **magnetar birth?** Also, it has not been demonstrated that FRB 121102 is representative of the overall FRB population. In fact, the repetition of its bursts is unique among all FRBs (Petroff et al. 2015), so it is natural to ask whether FRB 121102 is representative. An important first step is to demonstrate that the properties of FRB 121102 are consistent with the significant body of facts for the overall population (Macquart & Johnston 2015; Katz 2016). The repeating nature of FRB 121102 provides us with a sample of bursts covering a range of spectral properties, temporal properties, and luminosities that can be used to test its connection to the larger FRB population.

We can also assume that FRB 121102 is representative of all FRBs and use it to constrain the physical processes at play in the overall FRB population. In this case, we know that FRBs are apparently luminous, but if that is due to intrinsic processes, such as coherent, pulsar-like emission (Katz 2014; Luan & Goldreich 2014; Cordes & Wasserman 2016), or extrinsic effects like scintillation (Cordes et al. 2017). The paper presents an analysis of the spectral properties of VLA bursts implied by simultaneous observing at Effelsberg, GBT, AMI-LA, and Arecibo, including the first simultaneous detection of an FRB at two observatories. The repetition of FRB 121102 also has strong implications for calculations of their rate of occurrence (Connor et al. 2016a) and comparison to other classes of transient, such as superluminous supernovae (Tendulkar et al. 2017).

This paper opens by describing the multi-telescope observing campaign and a refined analysis of the nine VLA bursts. Next, we present the spectrum of a burst from FRB 121102 that was simultaneously detected by the VLA and Arecibo observatories. **Simulations of temporal statistics and luminosity distribution...** **New estimate of FRB rate and comparison to other transient populations** We close with a discussion of how the FRB 121102 burst spectra, host properties, burst rate estimates, and other properties inform new strategies for finding FRBs.

2. OBSERVATIONS

The data presented here were obtained from multiple programs and telescopes, but focuses on an observing campaign in August/September 2016. The central goal was to interferometrically localize FRB 121102 with the VLA in coordination with Arecibo Observatory, with others included on a best-effort basis. We coordinated observing between the VLA, Arecibo, Effelsberg, and AMI-LA telescopes, as shown in Figure 1. Below, we summarize these observations, with a focus on those conducted simultaneously with VLA burst detections from FRB 121102.

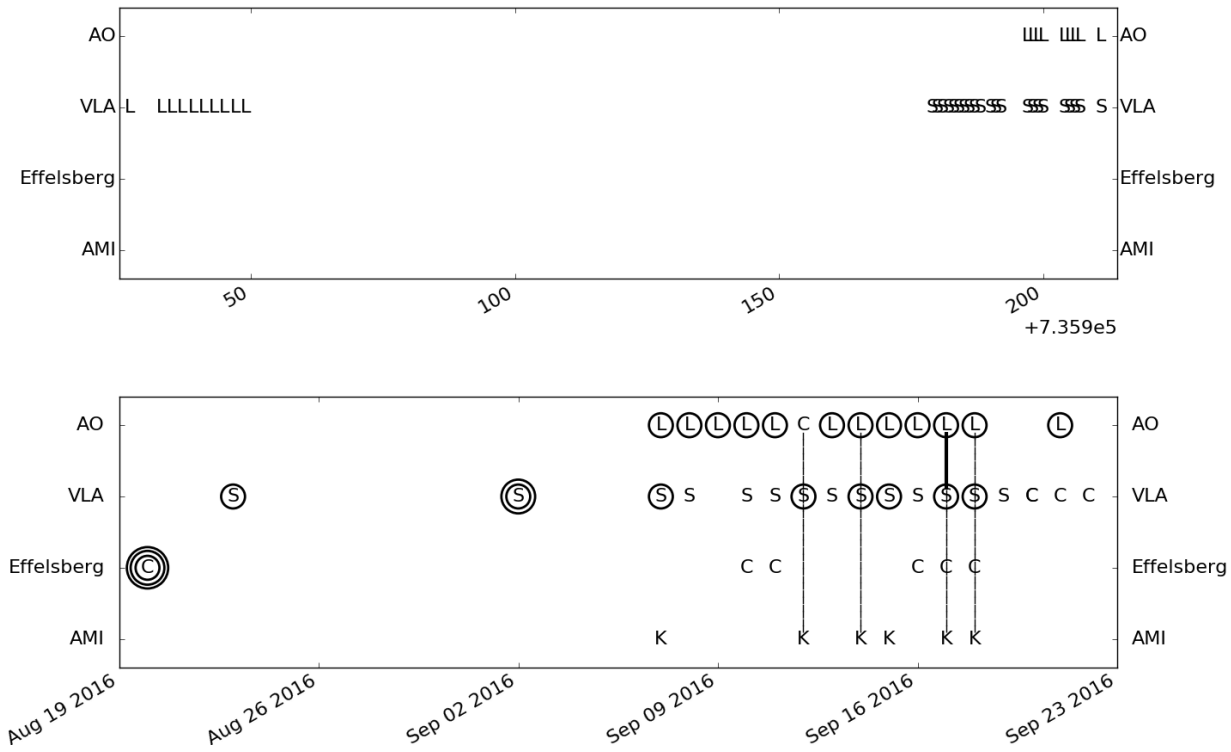

Figure 1. The top and bottom panels summarize the observing coverage and detections of FRB 121102 in the 2015 and 2016 campaigns. Symbols show days with observations and circles highlight observations that detected bursts from FRB 121102. Multiple circles indicate multiple burst detections, except for Arecibo, which typically has multiple detections per observing session (a detailed analysis is left for a future paper). The black dashed lines show the VLA burst detections with simultaneous coverage at other telescopes. The solid black line shows the simultaneous burst detection at VLA and Arecibo.

2.1. *VLA*

The FRB 121102 observing campaign started in late 2015 with a 10 hr campaign observed at 1.4 GHz in the compact D configuration. In April through May 2016, we conducted a 40 hr campaign at 3 GHz in the C and CnB configurations in coordination with Arecibo. We concluded with a 40 hr, coordinated campaign from August through September 2016 in the B configuration and during the move to the most extended A configuration. In the late-2016 campaign, the first 34 hours of VLA observations were made at 3 GHz, while the last 6 hours were observed at 6 GHz. This paper focuses on the data collected at 3 GHz, which includes all nine burst detections and is the widest bandwidth to have ever detected an FRB.

All VLA fast-sampled data were observed with 5 ms sampling, 256 channels, and dual-circular polarization (Law et al. 2015). The channel frequency width was set to maximize sensitivity to the known DM of FRB 121102with the largest total bandwidth. The total bandwidth at L (1.4 GHz), S (3 GHz), and C (6 GHz) bands was 256 MHz, 1024 MHz, and 2048 MHz, respectively. The 3 GHz data were recorded data in eight spectral windows with 32 channels each.

Observations in August and September were searched by a prototype version of *realfast*[1]. *realfast* is a real-time, fast imaging transient search system. The current prototype runs on CPU-based hardware that is normally dedicated to the VLA correlator; for this experiment, it runs the transient search pipeline software called *rtpipe* (`https://github.com/caseyjlaw/rtpipe`; Law et al. 2015). Images were formed for each integration with a DM grid of 0, 546, 556.9, 560, and 565 pc cm^{-3} and a time resampling grid of 5, 10, 20, 40, and 80 ms. This DM grid was chosen to maintain 90% sensitivity to the nominal DM range of 540–570 pc cm^{-3}, which includes the known FRB 121102 DM of 559 pc cm^{-3}. Gain calibration was made from observations of J0555+3948 by the "telcal" system, which uses phase-only calibration. A flux scale is calculated for each spectral window from an observation on xx (Bryan) and applied to all burst spectra.

[1] See `http://realfast.io`.

Burst detections and localizations were made within hours of data being recorded. The transient search starts when data are recorded and proceeds slower than real-time, so we refer to it as "quasi real-time". For each trial DM, integration, and time scale, we form an image and calculate the S/N ratio for the peak pixel in the dirty image. We empirically identified S/N thresholds of 6.4 and 7.4 as useful to capture data quality statistics and candidates for inspection, respectively. The higher threshold is relatively unlikely to be triggered by thermal noise in this configuration, so *realfast* generates a more detailed (and computationally intensive) candidate visualization that includes an image and spectrum. All visibilities are recorded so detailed analysis, including improved calibration and localization, can be conducted offline.

Computational notebooks to reproduce the transient detection, localization, and analysis presented here can be found at `https://github.com/caseyjlaw/FRB121102`. Time cut-out visibility data and calibration products are available at `https://doi.org/10.7910/DVN/TLDKXG`. Original visibility data are available under VLA program codes 16A-459 and 16A-496 and can be downloaded at `http://archive.nrao.edu`.

2.2. *Arecibo*

During the late-2016 campaign, Arecibo observed with the L-wide receiver using the PUPPI pulsar backend. The observational frequency range was 1.15 to 1.73 GHz and frequency resolution was 1.5625 MHz. We recorded total full Stokes polarization intensity spectra with time at a resolution of 10.24 μs. Each frequency channel was coherently dedispersed to 557 pc cm^{-3}, thereby eliminating intra-channel dispersion smearing. The full width at half maximum (FWHM) beam size at band center is 3.3′.

In total, twelve Arecibo observations had some simultaneous coverage with the VLA. Four of those observations were simultaneous with bursts detected with the VLA and one of those observations detected the same VLA burst. During the first VLA burst with Arecibo coverage (MJD 57643), the PUPPI system failed so data were recorded with xx (Jason?) at C band. No detection was made in those Arecibo data. Overall, there were many more bursts detected at Arecibo than with the VLA and a more detailed analysis of those bursts will be presented in a future paper.

2.3. *Effelsberg*

Effelsberg observations were conducted with the S60mm receiver at an observing frequency of 4.6 to 5.1 GHz. Total intensity spectra were recorded by the PFFTS backend in pulsar search mode with a time resolution of 65.5 μs and 128 frequency channels. The system equivalent flux density is 18 Jy and a FWHM beam size of 2.4′at 4.85 GHz.

Five Effelsberg observations had some simultaneous coverage with the VLA, of which two were simultaneous with VLA bursts. Unfortunately, due to a configuration error, a 100 MHz bandwidth filter centered at 4.85 GHz was in place for both of these sessions. The sensitivity was about two times worse than the nominal value. No burst was detected in either observation.

2.4. *AMI-LA*

We observed FRB 121102 with the Arcminute MicroKelvin Imager Large Array (AMI-LA; Zwart et al. 2008) for 3 hours each on four epochs starting at MJDs 57643, 57645, 57648, and 57649. Observations were made with the new digital correlator having 4096 channels across a 5 GHz bandwidth between 13–18 GHz with a 1 s integration time. The phase calibrator, J0518+3306, was observed every 12 minutes for about 1.5 minutes. The AMI-LA data were binned to eight 0.625 GHz channels and processed (RFI excision and calibration) with a fully-automated pipeline, AMI-REDUCE (e.g., Perrott et al. 2013). Daily measurements of 3C48 and 3C286 were used for the absolute flux calibration, which is good to about 10%.

We inspected the calibrated visibilities, and did not find any signal above 30 mJy in the 1s samples at and in the vicinity of the detected bursts. Concatenating and imaging the 12 hours of calibrated data with the CASA tasks *concat* and *clean* also does not yield any significant detection at the FRB location. Although the statistical 3σ upper limit is 60 μJy, extended mJy-level sources in the field cause sidelobe confusion (the AMI-LA angular resolution is $\sim$30″), and the actual upper limit is larger. We introduced artificial point sources at the FRB location using the CASA *sm* tool, and found that these sources can be recovered as long as their peak flux densities are more than $\sim 100\mu$Jy. Hence, we place an upper limit of $100 \pm 10\mu$Jy on any quiescent or possible radio flaring on $\sim$days timescales from the FRB. This limit is similar to the flux density measured by the VLA (Chatterjee et al. 2017).

3. RESULTS

3.1. *Multi-Observatory Burst Spectrum*

Four of the VLA bursts were observed simultaneously with Arecibo and AMI-LA (Figure 1). Of these, the burst on 57648 was detected by Arecibo at the same time (after correcting for the known DM of FRB 121102).

The Arecibo detection of this burst had a significance of xxσ (Jason).

Figure **to do** shows the dynamic spectrum formed from the phased VLA and Arecibo data... **Discuss dispersion correction, time alignment, chance of false association**

This simultaneous detection of a burst from roughly 1.2 to 3.5 GHz shows that some bursts emit over more than an octave of frequency. However, the other three...** ** is one of three VLA bursts with L-band coverage by Arecibo, which implies that those bursts had a smaller spectral width. However, all three VLA bursts with L-band Arecibo observations were relatively weak, so it is difficult to rule out L-band emission entirely. However, as described in §3.2.1, some of the VLA bursts peak within the band from 2.5 to 3.5 GHz, which implies a much smaller spectral coverage for typical bursts.

3.2. *VLA Bursts*

3.2.1. *Spectral Modeling*

We used two techniques to refine the analysis of the nine VLA radio burst spectra described in Chatterjee et al. (2017). First, we improved on the initial analysis by using a better calibration scheme and optimizing the detection significance over a fine grid of DM (ΔDM = 1 pc cm^{-3}). After calibration and flagging, the visibility phases were rotated to the best-fit location ((RA, Dec) = (05h31m58.70s, +33d08m52.5s); Chatterjee et al. 2017) to extract a Stokes I spectrum that maximizes the image S/N for each burst. Table 1 gives the resulting integrated burst flux density, image S/N, and Stokes V, while Figure 3 shows the Stokes I spectra. Generally, the burst spectra are characterized by a broad, Gaussian shape with inter-channel modulation as high as 100%.

To better understand the spectra, we extracted dynamic radio spectra (time versus frequency) for 2d modeling with the MCMC sampler *emcee* (Foreman-Mackey et al. 2013). These dynamic spectral were modeled as the product of a Gaussian shape (amplitude, center, width) and a temporal shape (start time, DM, and width). These 6-dimensional fits were sampled with 100 walkers taking 500 steps; typically, the first 200 steps were used to burn in the walkers and were ignored. A flat prior was used over all ranges with valid data, including a requirement that the Gaussian integral produce a detection significance higher than 8σ. To represent the strong inter-channel modulation, the model error was estimated as the maximum of the modeled flux and the measured, off-burst noise value (typically 70 mJy per 5 ms integration and 4 MHz channel).

The parameters for the best model of the dynamic spectrum are given in Table 1 and the resulting Gaussian model overlaid on Figure 3. The typical burst has a spectral width of 500 MHz. All but two of the best-fit Gaussians are centered inside the 3 GHz band and some appear contained by the 1 GHz wide band. This is consistent with previous detections of FRB 121102 by Arecibo, which showed quasi-broadband structure (Scholz et al. 2016) and large variation in the implied spectral index (Spitler et al. 2014). A detailed discussion of high-resolution FRB 121102 burst spectra seen by the Arecibo Observatory will be presented elsewhere (Hessels et al. 2017).

3.2.2. *Dispersion*

The initial VLA detections were made by searching a DM grid that allowed inter-DM sensitivity losses up to roughly 10% ($\Delta DM = 10$ pc cm^{-3} Cordes & McLaughlin 2003). In optimizing detection significance over a fine DM grid, we find optimal DM values range from 552 to 572 pc cm^{-3}. However, the uncertainty in the peak DM measurement is defined by the signal-to-noise of the burst and how this changes with DM.

Given that the apparent DM can potentially change due to intrinsic or extrinsic effects, we developed a more sophisticated system for modeling dispersion. We created a generative model to sample the likelihood distribution as a function of DM (Hogg et al. 2010). We use the Gaussian shape (see §3.2.1) along the spectral axis and apply a frequency-dependent delay for a given dispersion model. The likelihood is directly sampled by calculating the product of probabilities on a per-pixel basis of the 2-dimensional dynamic spectrum. Uncertainties in each pixel are drawn from a uniform Gaussian error distribution that is estimated from the data.

Does DM correlate with other spectral/flux properties?

Figure 4 compares the 95% confidence intervals on the DM for all nine VLA bursts to the range of DM previous observed (Spitler et al. 2014; Scholz et al. 2016). The DM confidence intervals are not consistent with each other or a single DM. This suggests that there are apparent DM changes between bursts, either due to intrinsic burst structure or actual changes to the DM column density. Elsewhere, we present high-resolution dynamic spectra at 1.4 GHz that show how intrinsic spectral structure can bias the apparent DM of individual bursts (Hessels et al. 2017). The FRB emission process has not yet been defined, so it is not clear how the intrinsic structure can bias DM as a function of frequency.

3.3. *Temporal Statistics*

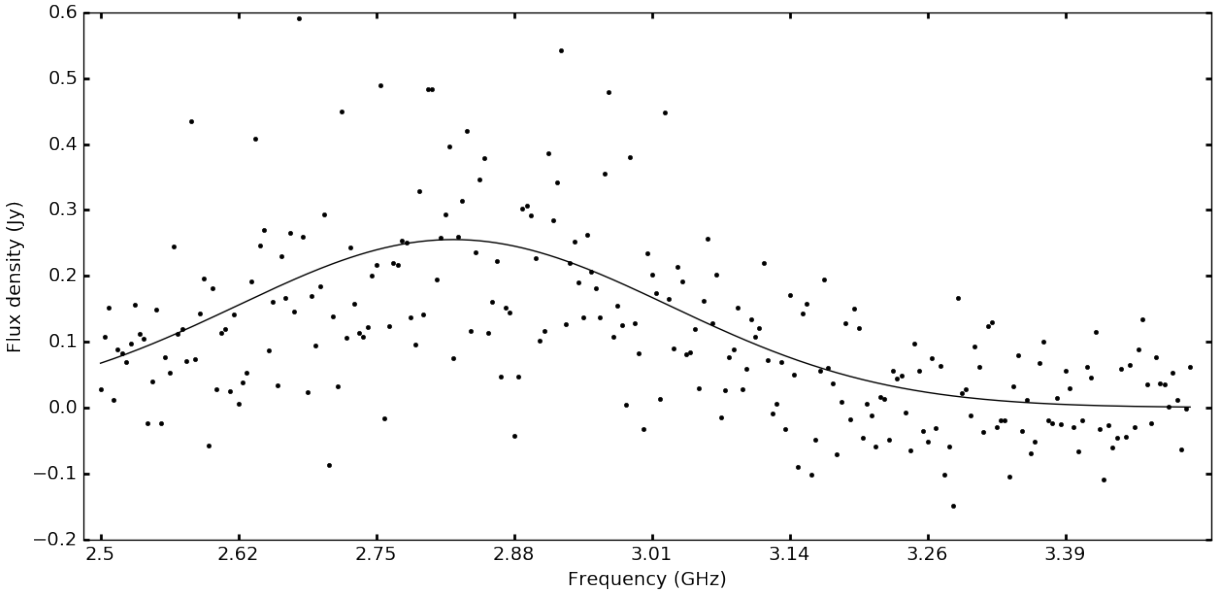

Figure 2. **Placeholder** Fill in with AO+VLA dynamic spectrum.

Table 1. Properties of Bursts from FRB 121102

Date (MJD)	$S_{I,int}$ (mJy)	Image S/N	E_{int} (10^{38} erg)	DM_{opt} (pc cm^{-3})	$S_{I,peak}$ (mJy)	Center (GHz)	FWHM (MHz)	S_V (mJy)
57623.74402686	194	38	11	562.1	690	2.8	290	+3
57633.67986367	1500	179	97	561.3	3350	3.2	510	–35
57633.69515938[a]	69	15	7	555.8	>430	<2.5	290	+2
57638.49937435	55	12	3	558.6	130	3.1	410	+5
57643.45730263	508	100	34	558.7	1170	2.8	510	–5
57645.42958602	64	13	4	555.9	170	2.8	380	+3
57646.46600650[a]	87	20	10	562.4	>420	<2.5	420	+1
57648.43691490[b]	111	25	7	557.4	260	2.8	470	+9
57649.45175697	167	36	12	559.9	290	3.0	690	+1

[a] Best-fit Gaussian is not centered in 3 GHz band, so spectral parameters are limits.

[b] Detected simultaneously with Arecibo between 1.15 and 1.73 GHz.

Geoff comments: – need to clarify that burst rate change is significant – not clear how significant nondetections are, since observational details not obvious yet

Burst detections were made very inhomogenously through the 2016 observing campaign and total 63 hours. In the early-2016 campaign, we observed for 30 hours at S-band and no bursts were detected. In the late-2016 observing campaign, nine bursts were detected in the last 27 hours of S-band observing. Overall, the data quality is uniform and high, so the inhomogeneous burst distribution shows that the burst detection probability was not stationary. Assuming that the burst detection probability follows a Poisson distribution, the nondetection in the first half of S-band limits the FRB rate to R < 0.1 hour^{-1} (95% confidence limit). The mean detection rate for S-band observing during the late-2016 campaign was R $= 0.33 \pm 0.1$ hour^{-1}.

There is weak evidence that the FRB 121102 burst rate decreased through the S-band observing in the late-2016 campaign. We modeled the event detection probability as a Poisson probability function, $P_i(\lambda)$, with rate parameter that evolves linearly in time relative to the first VLA burst $\lambda = a + b(\mathrm{MJD_i} - 57623)$. By directly sampling the joint probability distribution, $\prod_i P_i$, we

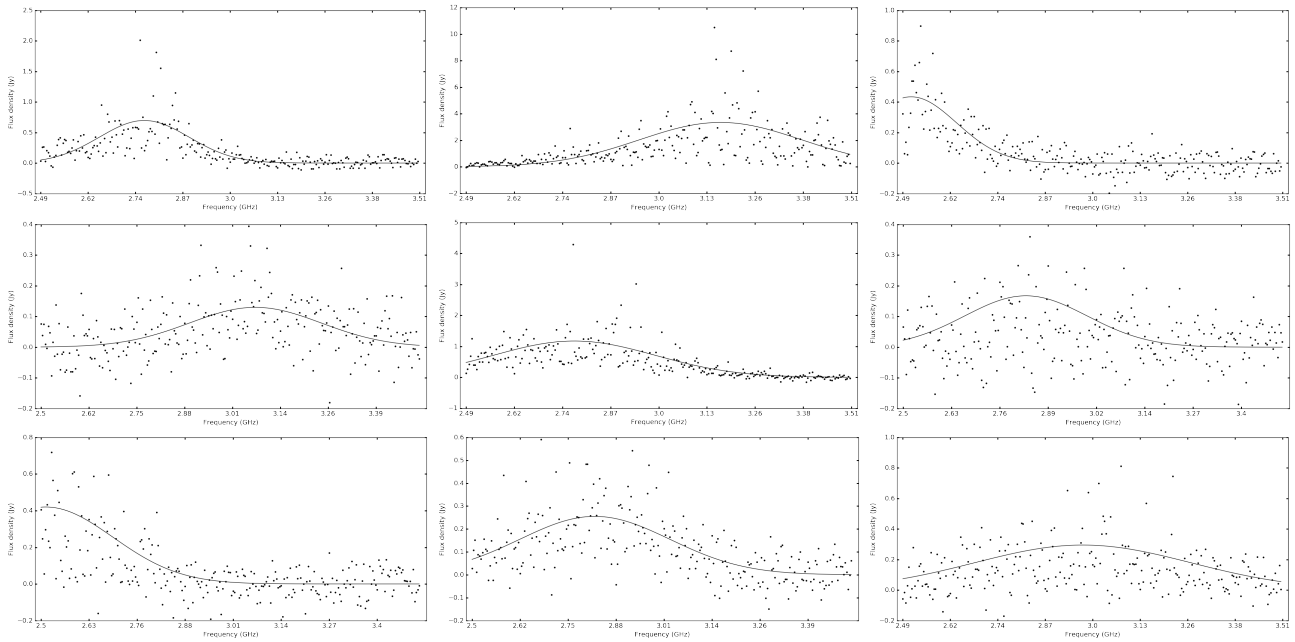

Figure 3. Spectra and best-fit model for nine bursts seen by the VLA from 2.5 to 3.5 GHz. Starting at the top left (moving right and then down), they correspond to bursts on MJDs 57623, 57633.68, 57633.70, 57638, 57643, 57645, 57646, 57648, and 57649. The solid line is a best-fit Gaussian model found through probabilistic modeling. Note that bursts are detected in 5 ms images generated from dedispersed visibilities.

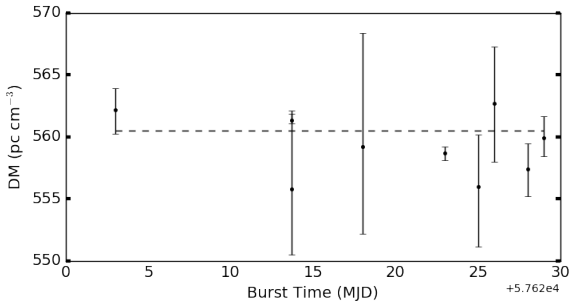

Figure 4. DM as a function of time for nine 3 GHz bursts detected by the VLA. The 95% confidence interval on DM is shown with a bar and the dahsed line shows the best-fit DM= 560.5 pc cm^{-3} inferred for Arecibo observations at 1.4 GHz (CITE: WEIRD).

can exclude a constant rate with ∼85% confidence. This weak constraint is consistent with the broader trend of a changing rate seen on month timescales by Arecibo.

During the late-2016 observing campaign, the typical observation lasted about two hours and was sampled with a 5 ms cadence. We used the Lomb-Scargle periodogram (Scargle 1982) to search for periodic structure over a wide range of timescales. The time series is calculated by binning the burst detection rate per 100 ms (always either 0 or 1, see also Palliyaguru et al. 2011). The spectral power calculated for periods between 0.8 and 80 s shows no power in excess of the typical 95% confidence bound estimated from shuffled data. We verified that simulating nine bursts drawn from a simple rotational model would produce excess power using this approach. However, it is difficult to put strong constraints on more complex rotational models (e.g., with wide pulse phase windows or glitches; Camilo et al. 2007; Archibald et al. 2013)

3.4. *Energy and Brightness Distribution*

Knowing the burst distance, we calculate their total energy by integrating flux in time and frequency (Table 1). Some VLA burst spectra seem to be contained by the 2.5 to 3.5 GHz band and most of them seem to have Gaussian envelopes that are well modeled by the emission within the 2.5 to 3.5 GHz band. Assuming that the Gaussian shape defines the emission window, the mean S-band flux density can be converted to a total energy with no further assumptions about their spectral properties. We proceed under this assumption here and discuss caveats is §4.

Figure 5 shows the FRB 121102 burst energy cumulative distribution and best-fit model. We modeled the differential energy distribution, $dN/d\log E$, as a Poisson probability distribution with a rate function $\lambda \propto E^{\alpha}$. Using a maximum likelihood technique, we estimate the best powerlaw index of $\alpha = -0.6^{+0.2}_{-0.4}$ (68% confidence interval), which is equivalent to a dN/dE powerlaw index of –1.6. This model assumes a completeness limit for a luminosity equivalent to an 8σ flux density limit. This

is consistent with the high and uniform data quality and the false positive rate in this observing campaign.

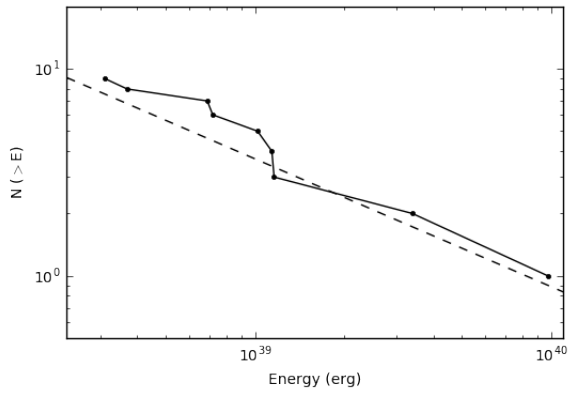

Figure 5. Dots and solid line show the FRB 121102 burst energy cumulative distribution. The dashed line shows the best fit from a maximum likelihood analysis using the powerlaw model $dN/d\log E \propto E^{\alpha}$. The 95% bounds on the best-fit powerlaw index is $\alpha = -0.6^{+0.2}_{-0.4}$.

3.4.1. *Spectral Autocorrelation*

Autocorrelation of the burst signal (both temporal and spectral) can be used to infer both intrinsic properties and modulation due to scintillation (Cordes et al. 2017). Figure 6 shows the spectral autocorrellation for the strongest burst (MJD 57633.68). The is no strong excess correlation near the channel resolution, which limits the correlation width to less than roughly 4 MHz. This is broadly consistent with expectations of Galactic diffractive scintillation bandwidth (3–9 MHz near 3 GHz Cordes & Lazio 2002).

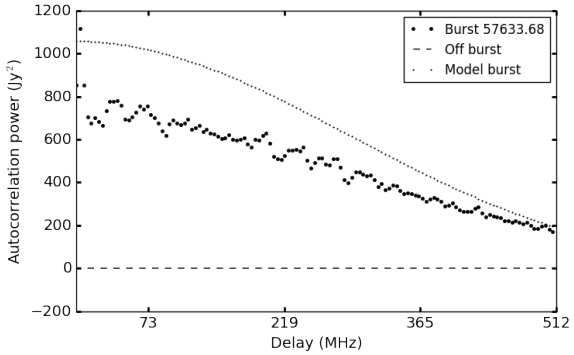

Figure 6. The spectral autocorrelation as a function of frequency for the burst from FRB 121102 at MJD 57633.68. The largest black dots show the autocorrelation for the data, smaller dots show the autocorrelation for the best Gaussian model, and dashed line shows the autocorrelation of an off-burst spectrum.

3.4.2. *Circular Polarization*

The VLA S-band recievers measure circular polarization, although for observing efficiency we choose not to include polarization calibration procedures. Constraints on circular polarization are possible since the gain calibrator is a well-known polarization calibrator with little Stokes V flux. In that case, the apparent circular polarization fraction is $(RR-LL)/(RR+LL)$, which for the most significant bursts is at most 3%. FRB 121102 was located 2.3′away from pointing center, where systematic effects have been measured as large as 3% (Perley et al 2016, VLA memo). Given that systematic effects dominate the apparent circular polarization, we conclude that the true fractional circular polarization is less than 3%.

4. DISCUSSION

4.1. *Emission Physics and Burst Energetics*

The refined analysis shows that FRB 121102 has even higher isotropic energies than previously reported, reaching energies $E_{\rm max} \approx 10^{40}$ erg. We now know that FRB 121102 is detectable with the VLA out to $z = 0.7$ and much farther with Arecibo. FRB 121102 has isotropic energies orders of magnitude higher than the strongest Crab pulsar pulses ($\sim 10^{35}$ erg) and comparable brightness temperatures ($T_b^{\rm Crab} \sim 10^{41}$ K versus $T_b^{\rm FRB121102} \sim 10^{38}$ K; Hankins et al. 2003; Katz 2014). While this emission is coherent and strongly beamed (Spitler et al. 2016; Hessels et al. 2017), the energy scale is still larger than any known Galactic radio transient and requires either a new process or dramatic scaling of known emission processes (Lyutikov et al. 2016; Cordes & Wasserman 2016).

– Self-organized criticality in the sun. energy powerlaw=-1.7 (Aschwanden 2011) – **Similarity to magnetar energy distribution**

Propagation effects (e.g., scintillation, scattering) can also modify the radio signal in a variety of ways and the duration of the emission in the source frame is not known (Cordes et al. 2016). Cordes et al. (2017) describe a model where plasma lensing near the source of an FRB can magnify radio emission by orders of mangitude. That model argues that the simultaneous appearance of a burst from 1.2 to 3.5 GHz requires a lens with the focal frequency be $\gtrsim 3.5$ GHz. This gives a constraint on the combination

$$\frac{\rm DM_0}{a_{\rm AU}^2}\frac{d_{sl}d_{lo}/d_{so}}{1\,\rm kpc} \gtrsim (3.5/39.1)^2$$

where DM_0, a, and d_* are the electron column density of the lens, size of the lens, and lensing distances, respectively. A lens placed at $d_{sl} \approx 1$ kpc is consistent with

typical properties of the interstellar medium. Lenses that are influenced by the source would be much nearer to the source $d \ll 1$ kpc, requiring large values of $\frac{\mathrm{DM}_0}{a^2_{\mathrm{AU}}}$.

4.2. *FRB Flux Distribution*

The Lorimer burst was surprising for its unusually large flux with a lack of lower-significance detections. As more FRBs have been detected, we continue to be surprised by their apparent brightness of FRBs (Ravi et al. 2016). This perception has been validated with analysis of the FRB cumulative fluence distribution, which when modeled as a powerlaw ($dN/dF \propto F^{\alpha}$) has an index $-0.5 < \alpha < -0.9$ (Vedantham et al. 2016; Li et al. 2016; Lawrence et al. 2016). For a uniform distribution of sources with a single luminosity, this index should be –1.5 (the "Euclidean" distribution, e.g., Lyutikov et al. 2016).

The energy distribution of FRB 121102 bursts has also produced some surprises. The nine bursts were detected with a wide range of significance (12 to 179σ) and the apparent burst energy distribution can be characterized as a powerlaw $dN/dE \propto E^{-1.6}$. If all FRBs luminosities are drawn from such a distribution, then their flux distribution will be determined by the underlying energy distribution and its interplay with redshift space distortions.

We tested this idea by simulating FRB populations and measuring the properties of a flux-limited subsample. First, we assume an FRB population that is uniformly distributed in space from redshifts $z1$ to $z2$. For each FRB source, we generate one FRB burst with a luminosity drawn from the FRB 121102 energy distribution and calculate its flux. We then select the brightest 15 (equal to the current sample size used in modeling; Vedantham et al. 2016) and fit a powerlaw to the dN/dF distribution. Typically, a large ($N > 10000$) population of such bursts is needed to avoid edge effects in the properties of the flux-limited subsample.

Figure 7 shows an example of an FRB population simulation with a dN/dE distribution like FRB 121102. We use visualizations like this to verify that the simulations are not affected by edge effects. We can also reproduce a Euclidean flux distribution for a standard candle-like luminosity distribution at low redshift and that distributions out to $z2 \sim 2$ have a flatter index ($\Delta\alpha \sim 0.2$) due to redshift space distortions.

To study how the input parameters affect the measured flux distribution, so we generated 100 populations to measure 68% confidence intervals on the cumulative flux distribution index. Figure 8 shows the result of several such measurements for input luminosity distribution index ranging from –2.2 to –1.2. Generally, the measured flux distribution index flattens as the input luminosity distributions flattens. The best constraint on the flux distribution index (Vedantham et al. 2016) requires an input energy distribution index between roughly –2.1 and –1.4, which is consistent with the measured energy distribution for FRB 121102. These simulations predict a mean a mean redshift between 0.9 and 1.8, which is in weak tension with the mean FRB redshift inferred from DM. For a mean total DM of 750 pc cm^{-3} and a mean host DM of 200 pc cm^{-3}, we expect a mean redshift of ~ 0.5 (Inoue 2004).

While the FRB 121102 burst energy distribution is consistent with the overall FRB population, this simulation ignores many observational biases (scattering, observing coverage) and the effects of galaxy evolution, which is likely significant over the range of redshifts to which FRB 121102is detectable (e.g., Ilbert et al. 2010). The burst energies are estimated from observations from 2.5 to 3.5 GHz, which may be a biased selection of all bursts or may not include all burst emission. If the simulation is revealing a connection between FRB 121102and the broader FRB population, it does not explain the physical mechanism that drives it. The burst energy distribution of the population could be dominated by intrinsic or extrinsic effects (Macquart & Johnston 2015; Spitler et al. 2016; Cordes et al. 2017). More FRB detections will improve the quality of this inference as sample variance drops, while more burst detetions from FRB 121102 will improve the measurement of the intrinsic energy distribution.

4.3. *Repetition*

The burst rate analysis presented in §3.3 shows that the detection probability of FRB 121102 is not stationary. As mentioned above, this could be caused by intrinsic events (e.g., magnetar outburst) or propagation effects. While a detailed analysis of temporal correlation will require more bursts and/or more sophistication, it is clear that FRB 121102 has significant correlation on short timescales (sometimes called a "red spectrum"; Connor et al. 2016a). Another way of stating this is that the detection of a burst improves odds of finding more bursts in near-future observations.

If this statistical property describes other FRBs, it weakens previous constraints on repetition (Petroff et al. 2015; Law et al. 2015). It is possible that other FRBs have repeating bursts, although calculating a limit requires knowing the temporal correlation function that defines the repetition. Repetition also implies that there are fewer phyiscal sources of FRBs than implied by the burst detection rate.

FRBs like SGRs? 2016ApJ...826..226K

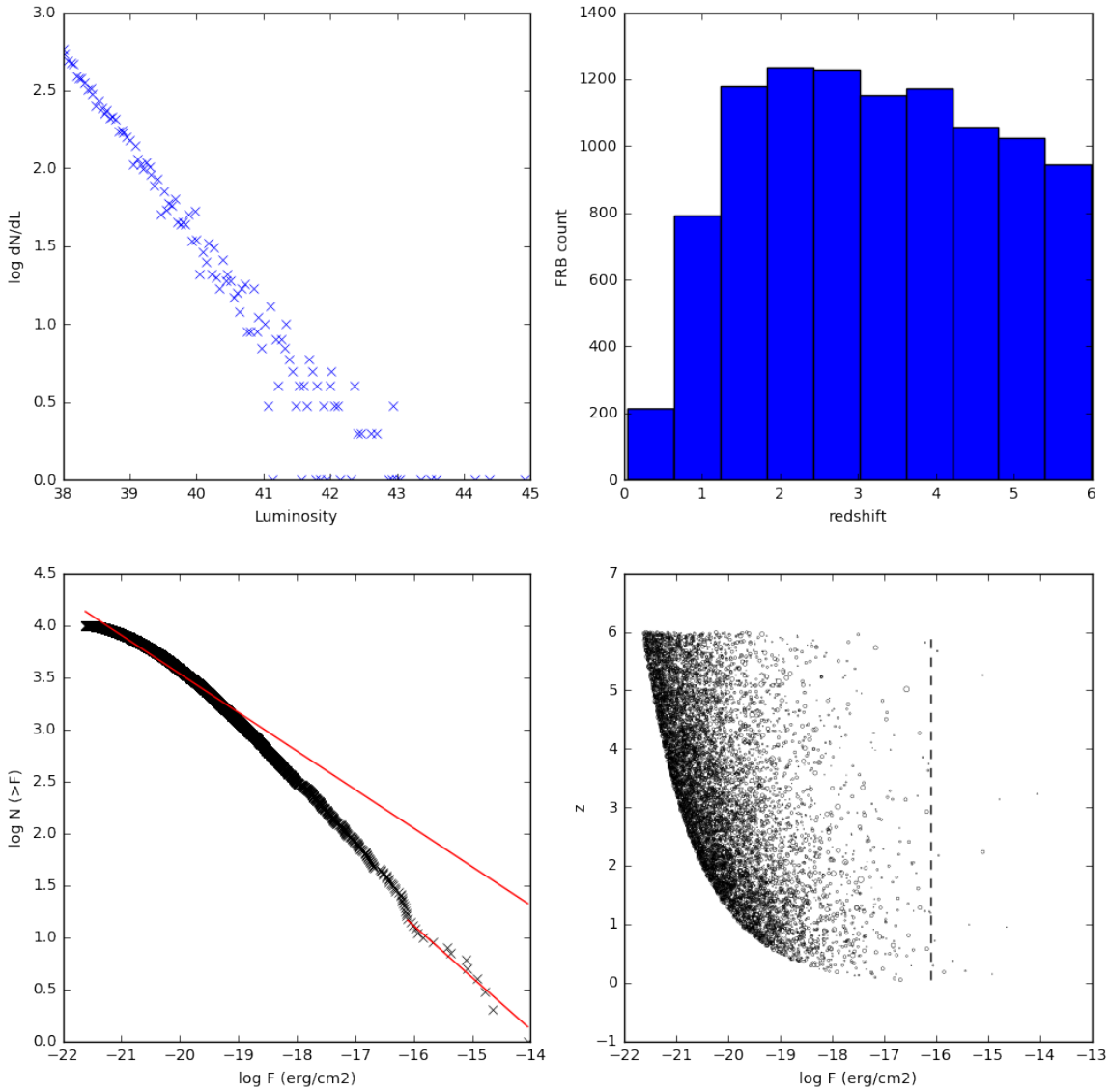

Figure 7. An example of a simulated FRB population. (Top left) The input luminosity distribution, which follows the FRB 121102 distribution of $dN/dE \propto E^{-1.6}$. (Top right) The input redshift space distribution of a uniform distribution of FRB sources. (Bottom left) The measured flux distribution of the simulation with red lines showing fits to the whole population and brightest 15 FRBs. (Bottom right) The flux-redshift distribution of the simulated population. The dahsed line shows the limiting flux that includes the brightest 15 sources.

4.4. *FRB Rate*

Sarah: can you update this as a per-SFR rate? Assuming that FRB 121102 is from the same population as the other FRBs, the measurement of a distance for the host of FRB 121102 allows us to re-evaluate the cosmic volume and event rate per galaxy for the FRB population. The estimated projected FRB rate R_p understates the true rate by a beaming fraction Ω_b ($\sim$10%; Tauris & Manchester 1998). For a comoving volume $V(z)$ and galaxy number density $\Phi(M)$, the rate per galaxy is $R_{FRB} = R_p/(\Omega_b \Phi(M) V(z))$.

The first such rate estimate was made by Thornton et al. (2013), who used the measured DM to estimate a characteristic distance for their sample of 4 FRBs. They assumed that all of the extragalactic component of the DM was caused by the IGM and scaled as $DM \approx z \times 1200 \mathrm{pc\ cm^{-3}}$ (Ioka 2003; Inoue 2004). They also calculated the number of galaxies by assuming a characteristic L_* galaxy (corresponding to stellar mass $M_* \approx 1011M$; Baldry et al. 2012).

add error bar? Our calculation differs in that we have better estimates of all three parameters. First, the projected FRB rate is now believed to be closer to

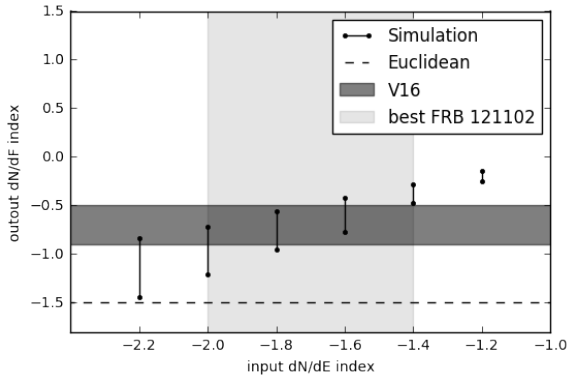

Figure 8. Scaling of apparent flux distribution index for given luminosity (or energy) distribution index.

2×10^3 sky^{-1}day^{-1} at high Galactic latitudes and flux densities brighter than 1 Jy ms (Lawrence et al. 2016; Champion et al. 2016; Rane et al. 2016). FRB 121102 is associated with a relatively small galaxy (5×10^7 Msun), which are roughly a factor of 100 more abundant ($\Phi(M) \approx 10^{-2}$Mpc^{-3}; Faber et al. 2007). Finally, the measured distance for FRB 121102 suggests that the extragalactic DM has comparable contributions from the IGM and host galaxy.

This reduces the characteristic distance by a factor of two and the volume by an order of magnitude. Considering these factors, we assume a characteristic redshift of the population that is twice that of FRB 121102 to estimate $R_{FRB} \approx 10^{-4}(0.1/\Omega_b)$galaxy^{-1}year^{-1}, which is two orders of magnitude lower than previously estimated (Thornton et al. 2013, assuming isotropic radiation;).

There are significant caveats to the comparison of this rate to the rates of other classes of transient. This isotropic FRB rate assumes a projected FRB rate at a single (observationally defined) flux limit and that no bursts repeat. Using this calculation with data from more sensitive telescopes, we might infer a higher rate. However, if we assume that FRB 121102 is representative of the overall FRB population, then more sensitive observations would be more likely to find repeating FRBs that would effectively depress the estimate of the underlying isotropic rate per source. In this model, these two effects partially cancel, although without a physical model it is difficult to say how well.

4.5. *Observing Strategies*

As discussed above, Connor et al. (2016a) note that the FRB repetition implies that the number of FRB-generating sources is smaller than implied by the number of bursts. In some scenarios, this means that there are areas on the sky that may contain no FRBs. Wide, shallow surveys are the preferred strategy for blind detection of FRBs. However, future efforts to localize FRBs are still most likely to succeed by targeting known FRBs to catch repetitions, assuming that all FRBs repeat. Finally, we note that the average spectral coverage of bursts from FRB 121102 are relatively narrow (< 1 GHz) and the coverage changes dramatically between bursts. Thus, the odds of detecting a burst will improve linearly with bandwidth for bandwidths wider than this characteristic scale.

5. CONCLUSIONS

Prior to being established as a cosmological source, the low Galactic latitude of FRB 121102 made it a somewhat compromised member of the FRB class. With its cosmological distance firmly established, FRB 121102 now serves as a new kind of standard by which FRBs are defined. That fact, combined with an abundance of data collected during its high activity state, allows us to think more generally about the physics of broader FRB population.

We presented the first multi-telescope detection (Arecibo and VLA) of an FRB. By detecting this burst from 1.2 to 4.5 GHz, we have demonstrated that some bursts have broad spectral structure. However, three other VLA bursts are undetected by Arecibo. That, combined with the measurement of spectra within the VLA band, suggest that the typical burst has a characteristic Gaussian spectral shape with width $\sim$ 500 MHz.

Flux/lum distribution

Analysis of the VLA burst times shows that the burst rate is highly variable. This shows that past constraints on FRB repetition are weaker than previously inferred. The combination of relatively narrow spectral structure, flat energy and flux distributions, and variable burst rate suggests that repeated observations, wide bandwidth, and large instantaneous field of view all improve the chance of detection.

New, arcsecond-scale localizations will continue to be highly informative, given that FRB hosts may be faint and can confuse the inference of a properties of the intergalactic medium (Deng & Zhang 2014). FRB 121102 was localized within hours by a prototype version of *realfast*, but an expanded *realfast* system is now under construction. This platform will search a TB/hour data stream in real time in parallel with ongoing VLA observations, potentially detecting and localizing multiple FRBs per year. Sarah: any refinement to this statement? VLASS+*realfast*?

ACKNOWLEDGEMENTS

The National Radio Astronomy Observatory is a facility of the National Science Foundation operated un-

der cooperative agreement by Associated Universities, Inc.. This research made use of Astropy, a community-developed core Python package for Astronomy (Astropy Collaboration, 2013). CJL is supported by the University of California Office of the President under Lab Fees Research Program Award 237863 and NSF award **number**. MAM is supported by NSF award #1458952. KPM's research is supported by the Oxford Centre for Astrophysical Surveys which is funded through the Hintze Family Charitable Foundation. AS gratefully acknowledges support from the European Research Council under grant ERC-2012- StG-307215 LODESTONE. The AMI-LA telescope gratefully acknowledges support from the European Research Council under grant ERC-2012- StG-307215 LODESTONE, the UK Science and Technology Facilities Council (STFC) and the University of Cambridge.

REFERENCES

Archibald, R. F., et al. 2013, Nature, 497, 591
Aschwanden, M. J. 2011, SoPh, 274, 99
Baldry, I. K., et al. 2012, MNRAS, 421, 621
Camilo, F., et al. 2007, ApJ, 663, 497
Champion, D. J., et al. 2016, MNRAS, 460, L30
Chatterjee, S., et al. 2017, Nature, 541, 58
Connor, L., Pen, U.-L., & Oppermann, N. 2016a, MNRAS, 458, L89
Connor, L., Sievers, J., & Pen, U.-L. 2016b, MNRAS, 458, L19
Cordes, J. M., & Lazio, T. J. W. 2002, ArXiv Astrophysics e-prints
Cordes, J. M., & McLaughlin, M. A. 2003, ApJ, 596, 1142
Cordes, J. M., & Wasserman, I. 2016, MNRAS, 457, 232
Cordes, J. M., Wharton, R. S., Spitler, L. G., Chatterjee, S., & Wasserman, I. 2016, ArXiv e-prints
Cordes et al. 2017, in prep
Deng, W., & Zhang, B. 2014, ApJL, 783, L35
Dokuchaev, V. I., & Eroshenko, Y. N. 2017, ArXiv e-prints, 1701.02492
Faber, S. M., et al. 2007, ApJ, 665, 265
Foreman-Mackey, D., Hogg, D. W., Lang, D., & Goodman, J. 2013, PASP, 125, 306
Hankins, T. H., Kern, J. S., Weatherall, J. C., & Eilek, J. A. 2003, Nature, 422, 141
Hessels et al. 2017, in prep
Hogg, D. W., Bovy, J., & Lang, D. 2010, ArXiv e-prints
Ilbert, O., et al. 2010, ApJ, 709, 644
Inoue, S. 2004, MNRAS, 348, 999
Ioka, K. 2003, ApJL, 598, L79
Kashiyama, K., & Murase, K. 2017, ArXiv e-prints, 1701.04815
Katz, J. I. 2014, PhRvD, 89, 103009
—. 2016, Modern Physics Letters A, 31, 1630013
Kulkarni, S. R., Ofek, E. O., Neill, J. D., Zheng, Z., & Juric, M. 2014, ApJ, 797, 70
Law, C. J., et al. 2015, ApJ, 807, 16
Lawrence, E., Vander Wiel, S., Law, C. J., Burke Spolaor, S., & Bower, G. C. 2016, ArXiv e-prints
Li, L., Huang, Y., Zhang, Z., Li, D., & Li, B. 2016, ArXiv e-prints
Lorimer, D. R., Bailes, M., McLaughlin, M. A., Narkevic, D. J., & Crawford, F. 2007, Science, 318, 777
Luan, J., & Goldreich, P. 2014, ApJL, 785, L26
Lyutikov, M., Burzawa, L., & Popov, S. B. 2016, MNRAS, 462, 941
Macquart, J.-P., & Johnston, S. 2015, MNRAS, 451, 3278
Marcote, B., et al. 2017, ApJL, 834, L8
McQuinn, M. 2014, ApJL, 780, L33
Metzger, B. D., Berger, E., & Margalit, B. 2017, ArXiv e-prints,1701.02370
Palliyaguru, N. T., et al. 2011, MNRAS, 417, 1871
Perrott, Y. C., et al. 2013, MNRAS, 429, 3330
Petroff, E., et al. 2015, MNRAS, 454, 457
Planck Collaboration et al. 2016, A&A, 594, A13
Rane, A., Lorimer, D. R., Bates, S. D., McMann, N., McLaughlin, M. A., & Rajwade, K. 2016, MNRAS, 455, 2207
Ravi, V., et al. 2016, ArXiv e-prints
Scargle, J. D. 1982, ApJ, 263, 835
Scholz, P., et al. 2016, ArXiv e-prints
Spitler, L. G., et al. 2014, ApJ, 790, 101
—. 2016, Nature, 531, 202
Tauris, T. M., & Manchester, R. N. 1998, MNRAS, 298, 625
Tendulkar, S. P., et al. 2017, ApJL, 834, L7
Thornton, D., et al. 2013, Science, 341, 53
Vedantham, H. K., Ravi, V., Hallinan, G., & Shannon, R. M. 2016, ApJ, 830, 75
Zhang, B. 2017, ArXiv e-prints, 1701.04094